Available online at www.sciencedirect.com

ScienceDirect

Geochimica et Cosmochimica Acta 268 (2020) 142–159

Geochimica et Cosmochimica Acta

www.elsevier.com/locate/gca

BayMBT: A Bayesian calibration model for branched glycerol dialkyl glycerol tetraethers in soils and peats

Emily Dearing Crampton-Flood [a,*], Jessica E. Tierney [b], Francien Peterse [a], Frédérique M.S.A. Kirkels [a], Jaap S. Sinninghe Damsté [a,c]

[a] Utrecht University, Department of Earth Sciences, Princetonlaan 8A, Utrecht 3584CB, the Netherlands
[b] University of Arizona, Department of Geosciences, 1040 E 4th St, Tucson, AZ 85721, United States
[c] NIOZ Royal Netherlands Institute for Sea Research, Department of Marine Microbiology and Biogeochemistry, and Utrecht University, Den Burg 1790 AB, Texel, the Netherlands

Received 7 February 2019; accepted in revised form 26 September 2019; available online 8 October 2019

Abstract

Accurate temperature records for the deep geological past are a vital component of paleoclimate research. Distributional changes of branched glycerol dialkyl glycerol tetraether (brGDGT) lipids in geological archives including paleosoils are a promising indicators to infer past continental air temperatures. However, the 'orphan' status of the brGDGTs, the potential effect of temperature-independent parameters on their relative distribution, and the uneven geographical distribution of the soils used for calibration contribute to the high uncertainty of brGDGT-based transfer functions (root mean squared error, RMSE: ±5 °C). Here, we expand the soil dataset from the previous calibration(s) with new and published soil data. We use Bayesian statistics to calibrate the relationship of the 5-methyl brGDGTs (MBT'_{5Me}) and mean annual air temperature (MAAT). The addition of soils from warm (>28 °C) environments from India substantially increases the upper limit of the Bayesian calibration (BayMBT) from 25 to 29 °C, aiding in the generation of temperature records for past greenhouse climates, such as the Eocene. The BayMBT model also effectively minimizes the structured MAAT residuals prevalent in previous calibrations, therefore giving the opportunity to explore confounding factors on the calibration. We formulate a set of alternative calibration models to test the effect of specific environmental parameters and show that soils at mid-latitudes with temperature seasonalities >20 °C are not well described by the BayMBT model. We find that the MBT'_{5Me} index is best correlated to the average temperature of all months >0 °C, called the $BayMBT_0$ model. This finding supports the hypothesis that brGDGT production ceases or slows down in the winter months. However, a persistent feature of the BayMBT model and previous calibrations is the significant scatter at mid-latitudes, which is speculatively linked with a possible increase in diversity of microbial brGDGT-producing communities in these locations.

Keywords: brGDGTs; Paleothermometry; Bayesian statistics

1. INTRODUCTION

The generation of high-fidelity temperature records for both recent and deep time is an important component of paleoclimate research. The distribution of branched glycerol dialkyl glycerol tetraethers (brGDGTs; Sinninghe Damsté et al., 2000) in soils is a promising proxy for conti-

* Corresponding author at: School of Earth and Environmental Sciences, The University of Manchester, Williamson Building, M13 9QQ Manchester, United Kingdom.
E-mail address: emily.dearingcrampton-flood@manchester.ac.uk (E. Dearing Crampton-Flood).

https://doi.org/10.1016/j.gca.2019.09.043
0016-7037/

nental temperatures (Weijers et al., 2007a). The basic chemical structure of the brGDGTs consists of two linear (C_{28}) alkyl chains linked to the glycerol moieties on either end via ether bonds. These alkyl chains contain a variable number of methyl branches (2–4; at C-13 and C-16 and, additionally, C-5 and C-6) and cyclopentane moieties (0–2), the latter formed through internal cyclisation (Sinninghe Damsté et al., 2000; Weijers et al., 2006). The stereochemistry of the glycerol moieties of brGDGTs confirms a bacterial origin (Weijers et al., 2006), and indicates that the producers may be heterotrophic facultative aerobes derived from Acidobacteria (Weijers et al., 2009, 2010). Indeed, the simplest brGDGT structure, Ia (Appendix A), was identified in two species of Acidobacteria (Sinninghe Damsté et al., 2011). Furthermore, Acidobacteria from the subdivisions 1, 3, 4, and 6 contain *iso*-diabolic acid, a presumed building block of brGDGTs, sometimes additionally methylated at the same position as in the GDGTs (Sinninghe Damsté et al., 2011, 2018). However, the origin of brGDGTs other than Ia remains enigmatic, even after an extensive screening of cultured members of the Acidobacteria (see Sinninghe Damsté et al., 2018, for an overview).

Weijers et al. (2007a) discovered a link between the degree of methylation of brGDGTs (MBT; methylation of branched GDGTs) with temperature and pH of soils. The authors also observed that the number of cyclopentane moieties is related to soil pH (CBT; cyclisation of branched GDGTs) and formulated an empirical proxy (MBT/CBT) to reconstruct past MAAT and soil pH. Application of these empirical relations on brGDGTs in sedimentary archives has resulted in continental temperature records for various locations and geological timescales, up to the Paleocene (Weijers et al., 2007b, c; Ballantyne et al., 2010; Inglis et al., 2017). Marine sedimentary records from locations nearby the mouth of large rivers are especially suited for these kinds of reconstructions since they receive eroded soil material from the entire river basin, thereby integrating the brGDGT-derived temperature signal. Subsequent studies revealed that brGDGTs may also derive from aquatic sources (e.g. Peterse et al., 2009a; Sinninghe Damsté et al., 2009; Tierney and Russell, 2009; Zell et al., 2013a, b; Zell et al., 2014a, b; De Jonge et al., 2014a; Sinninghe Damsté, 2016; Weber et al., 2015, 2018), complicating the application of the brGDGT paleothermometer in geological archives where a mixed aquatic and soil input (e.g. Dearing Crampton-Flood et al., 2018; Warden et al., 2018) is more likely compared to loess-paleosol sequences (e.g. Peterse et al., 2011).

An improvement in the chromatographic analysis of brGDGTs led to the discovery of brGDGT isomers with a methyl group located at the C-6 rather than the C-5 position of the alkyl chain (De Jonge et al., 2013, 2014b). Reanalysis of soils with this method resulted in an improved form of the MBT index: the MBT'_{5Me} index, which recognizes that only the distribution of 5-methyl brGDGTs respond to temperature, whereas the relative abundance of 6-methyl brGDGTs is related to the pH of the soil (De Jonge et al., 2014b). The discovery of the 6-methyl brGDGTs also led to the recognition of brGDGT production in rivers (De Jonge et al., 2014a) and how this production can affect brGDGT distributions in shelf sediments (De Jonge et al., 2015).

Recent research into the microbial diversity and community composition of global soil datasets suggests that soil pH and MAAT are the dominant controls on bacterial communities in a wide range of locations and biomes (Delgado-Baquerizo et al., 2017; Oliverio et al., 2017). Despite the strong link of soil-derived brGDGTs with temperature and soil pH, it is reasonably likely that also other factors, such as temperature seasonality, precipitation, and microbial community composition, affect their relative distribution (Weijers et al., 2007a; Peterse et al., 2012; Menges et al., 2014; Ding et al., 2015; Dang et al., 2016). However, due to the limited information on the biological sources of brGDGTs, pure culture experiments with brGDGT producers have not been performed to test this. Instead, the direct influence of temperature on brGDGTs in soils has been studied in geothermally heated soils, altitudinal transects, or mesocosm experiments (e.g. Sinninghe Damsté et al., 2008; Peterse et al., 2009b; Huguet et al., 2014; Chen et al., 2018; Martínez-Sosa and Tierney, 2019).

Four practical challenges exist for the application of the brGDGT temperature proxy in its current form. Firstly, the proxy becomes 'saturated' (i.e. $MBT'_{5Me} = 1$) at temperatures > 25 °C, limiting the application of the proxy in past greenhouse climates (De Jonge et al., 2014b; Naafs et al., 2017a). Secondly, there is evidence for soil moisture content exerting an effect on the methylation patterns of brGDGTs in arid areas, which are dominated by 6-methyl brGDGTs and are associated with large errors in reconstructed temperatures, even using the MBT'_{5Me} index which is based solely on the distribution of 5-methyl brGDGTs (Dang et al., 2016). In light of this observation, the most recent calibration of MBT'_{5Me} with temperature (Naafs et al., 2017a) imposed a cut-off based on the relative proportion of 6-methyl brGDGTs expressed as the Isomer Ratio (IR; De Jonge et al., 2014a):

$$IR = \frac{[IIa'] + [IIb'] + [IIc'] + [IIIa'] + [IIIb'] + [IIIc']}{[IIa'] + [IIb'] + [IIc] + [IIIa'] + [IIIb'] + [IIIc'] + [IIa] + [IIb] + [IIc] + [IIIa] + [IIIb] + [IIIc]} \quad (1)$$

Naafs et al. (2017a) removed all soils with IR > 0.5, excluding about 50% of the dataset. The authors proposed to use this cut-off as a method of screening environmental archives for the applicability of the proxy. However, this approach is challenging to apply marine sedimentary archives with mixed brGDGT sources. The third challenge

is that some of the previous calibration models (e.g. De Jonge et al., 2014b) tend to under-predict temperatures for warmer soils and over-predict for colder soils. This is caused by "regression dilution", where random measurements in the independent variable (in this case the MBT'_{5Me} index) cause a bias of the regression slope coefficient toward zero (referred to as slope attenuation). This can be alleviated by using Deming regression (for details see Naafs et al., 2017a), but this technique requires an *a priori* assumption of the analytical error for MBT'_{5Me} and MAAT, which are not well constrained. The fourth and probably most important challenge is related to the relatively high root mean squared error (RMSE) of the proxy and especially the large difference of the predicted and observed MAAT values (i.e. MAAT residuals) at mid-latitudes (30–50°; e.g. Fig. 11 in De Jonge et al., 2014b). This may reflect (1) a seasonal bias, as brGDGT production might increase during the warmer summer months (e.g. Weijers et al., 2011; Deng et al., 2016); (2) the heterogeneous nature of soils, which may affect the representability of samples in soil datasets; (3) variation in the difference between soil temperatures affecting brGDGT distributions directly and air temperature; and/or (4) variation in the microbial diversity of brGDGT producers. To take some of these considerations into account, Naafs et al. (2017a) considered in their brGDGT soil calibration growing degree days above freezing (GDD), a measure of annual soil heat accumulation, and the moisture index (MI) of soils as potentially better indicators for the conditions that soil bacteria experience. A new transfer function including these parameters resulted in a slightly reduced RMSE (4.1 °C) and improved model fit ($R^2 = 0.76$). Nevertheless, the error in brGDGT-based temperature estimates is still substantial, demonstrating that we still do not have a full understanding of the factors influencing brGDGT methylation.

Here, we use Bayesian statistics to construct a general calibration model for the MBT'_{5Me} index vs. MAAT that propagates observational and parametric uncertainties. Previous calibrations using ordinary least squares (OLS) regression and Deming regression are limited in that the MBT'_{5Me} was treated as the independent variable. This is because the goal of the proxy calibration is to predict temperatures (MAAT, i.e. dependant variable) from a given MBT'_{5Me} index value. However, given the scatter in the MBT'_{5Me}-MAAT relationship, this will result in severe regression dilution if using OLS due to the random measurement error in MBT'_{5Me} index, and mild dilution in the Deming case, if the uncertainty in the observations is underestimated. With the Bayesian approach, the MBT'_{5Me} index can be treated as the dependent variable in the calibration model, respecting the intuitive (etiological) reasoning of the relationship between MBT'_{5Me} and MAAT (i.e. brGDGT-producing bacteria respond to changes in temperature, not the other way around). Using this approach an ensemble of possible regression parameters are obtained that are able to account for errors in the measurement of both MAAT and MBT'_{5Me}. A second application of Bayes' rule can then be used to invert the relationship between the two variables, in order to predict MAAT values from a given MBT'_{5Me} value, i.e. the goal of a paleoclimatological study. In addition, the mounting evidence for controls other than MAAT on the brGDGT temperature proxy calls for an exploration of the variance in MBT'_{5Me} indices that is not explained by MAAT. In this paper, we also explore patterns in the residuals of the Bayesian calibration model with regard to presumably confounding environmental parameters, namely: temperature seasonality, mean annual precipitation (MAP), precipitation seasonality, and soil pH. We also explore other Bayesian calibration models that take these environmental parameters into account and discuss their suitability for certain datasets.

2. METHODS

2.1. Surface soil dataset

The soil brGDGT data used in this study are listed in Table 1. All analyses were performed using high-resolution chromatographic methods separating 5-methyl and 6-methyl brGDGT isomers (De Jonge et al., 2013). For this study, 66 new soils from India, Russia, New Zealand, and China were added to the global soil dataset of De Jonge et al. (2014b) to extend the spatial distribution of the calibration dataset (Fig. 1A). Published soil data from China (Ding et al., 2015; Xiao et al., 2015; Yang et al., 2015; Lei et al., 2016; Wang et al., 2016) and data from 96 globally distributed peatlands (Naafs et al., 2017b) were also added to the dataset. All newly obtained soils were freeze-dried, homogenized, and extracted (3x) using dichloromethane (DCM):methanol (9:1, *v*/*v*) with an accelerated solvent extractor (ASE 350, Dionex™) for 5 min at 100 °C and 7.6×10^6 Pa. The extracts were dried under a gentle stream of N_2 prior to separation into apolar and polar fractions using an activated Al_2O_3 column with hexane:DCM (9:1, *v*/*v*) and DCM:methanol (1:1, *v*/*v*). An internal standard (IS, $GTGT_{46}$) was added to the polar fraction (Huguet et al., 2006). For GDGT analysis, the polar fraction was dried under N_2, re-dissolved in hexane:isopropanol 99:1 (*v*/*v*), and filtered through a 0.45 μm PTFE filter. Samples were analysed with an Agilent 1260 Infinity ultra high performance liquid chromatography (UHPLC) coupled to an Agilent 6130 single quadrupole mass detector using the method of Hopmans et al. (2016). The system consists of two silica Waters Acquity UPLC BEH Hilic (1.7 μm, 2.1 mm × 150 mm) columns maintained at 30 °C, with a guard column of the same material preceding the first column. GDGTs were separated using isocratic elution at 0.2 ml/min, starting with 82% A and 18% B for 25 min, followed by a linear gradient to 70% A and 30% B for 25 min, where A = hexane and B = hexane:isopropanol 9:1. Sample injection volumes were 10 μL. GDGTs were ionized using atmospheric pressure chemical ionization with the following source conditions: gas temperature 200 °C, vaporizer temperature 400 °C, drying gas (N_2) flow 6 L/min, capillary voltage 3500 V, nebulizer pressure 25 psi, corona current 5.0 μA.

BrGDGTs were identified using selected ion monitoring (SIM) mode using detection of the $[M-H]^+$ ions at *m*/*z* 1050, 1048, 1046, 1036, 1034, 1032, 1022, 1020, 1018. The

Table 1
Number, location, and references for soils and peats used for the Bayesian calibration of MBT'_{5Me} and gridded MAAT.

Number of soils/peats*	Location	Reference(s)
229	Globally distributed	Weijers et al. (2007a), Peterse et al. (2012), De Jonge et al. (2014b)
46	India	This study
4	Russia/Siberia	This study
1	New Zealand	This study
15	China	This study
27	China	Xiao et al. (2015)
26	China	Yang et al. (2015)
27	China	Ding et al. (2015)
44	China	Lei et al. (2016)
148	China	Wang et al. (2016)
96*	Globally distributed	Naafs et al. (2017b)
N = 663		

* Indicates peats.

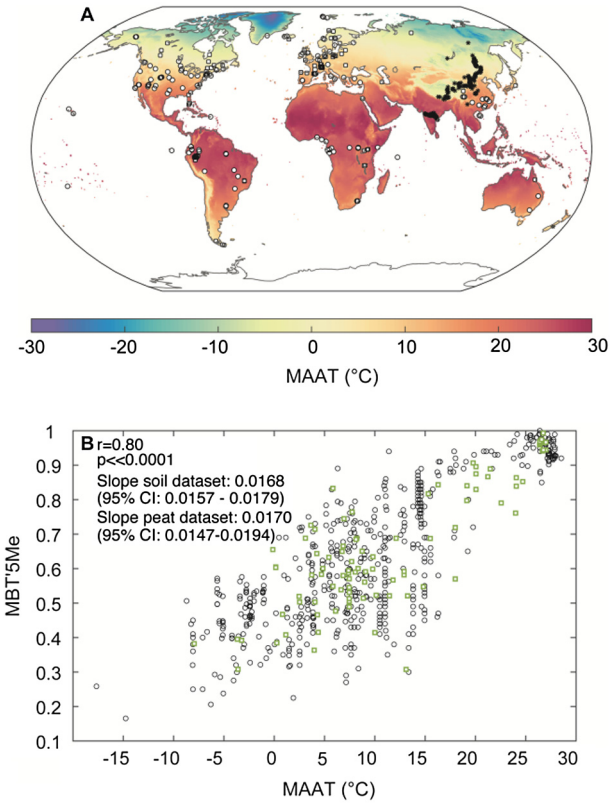

Fig. 1. (A) Geographical location of the soils and peats used in the study. Soils analysed for the previous calibration are represented by circles (De Jonge et al., 2014b), soils added to the dataset in this study are represented by black stars (Xiao et al., 2015; Yang et al., 2015; Lei et al., 2016; Ding et al., 2015; Wang et al., 2016; this study), and peats are represented by squares (Naafs et al., 2017b). (B) Plot of measured MBT'_{5Me} indices for global soils (black circles) and peats (green squares) versus MAAT. Pearson correlation coefficients (r) and p values are shown. Gridded MAAT is obtained from the CRU TS v. 3.24.01 dataset (Harris et al., 2014). (For interpretation of the references to color in this figure legend, the reader is referred to the web version of this article.)

internal standard was detected at *m/z* 744. Samples were integrated manually using the Chemstation software B.04.02.

2.2. The MBT'_{5Me} index

We used MBT'_{5Me} rather than the MAT_{mr} function to infer MAAT from the distribution of brGDGTs, as the MBT'_{5Me} incorporates only 5-methyl brGDGTs, which have the strongest relationship with MAAT (De Jonge et al., 2014b), and is a straightforward index for the degree of methylation, the presumed biophysical response to temperature. The formula for MBT'_{5Me} (De Jonge et al., 2014b) is defined as:

$$MBT'5Me = \frac{Ia + Ib + Ic}{Ia + Ib + Ic + IIa + IIb + IIc + IIIa} \quad (2)$$

2.3. Environmental parameters

Due to the scarcity of in situ soil temperature logger data, MBT'_{5Me} indices in this study were compared to mean annual air temperatures (MAAT). Nearest gridded MAAT to the soil sampling sites (determined by chordal distance) were extracted from the 0.5° gridded CRU TS v. 3.24.01 dataset (Harris et al., 2014). As the turnover time for brGDGTs in soils is on the order of decades (Peterse et al., 2010; Weijers et al., 2010, 2011; Huguet et al., 2014), we used monthly or annual mean temperatures averaged over January 1901 to December 2015. The chordal distance between the MBT'_{5Me} observations and the centroid of the nearest MAAT observation is smaller than 40 km for all sites (median 21 km; Appendix C), except for one case: USA-10; Hawaii, where it is 48 km. Using this method to estimate MAAT leads to a homogeneous temperature collection, which is preferable to compilation using different datasets/weather stations, as was done in previous work (Weijers et al., 2007a; Peterse et al., 2012; De Jonge et al., 2014b). Nevertheless, comparison of the gridded MAAT with the instrumental MAAT from the dataset of De Jonge et al. (2014b) shows a good correlation ($r = 0.90$; $p < 0.0001$).

Gridded precipitation data (MAP) for each month was also taken from the CRU TS v. 3.24.01 dataset (Harris et al., 2014). Extraction of the precipitation data and assignment to the MBT'_{5Me} values followed the same method as above.

In case that two or more soils fall within the same grid-box used to estimate MAAT, average MBT'_{5Me} values were taken to avoid weighting the regression exercises (cf. Tierney and Tingley, 2018), leaving the total number of soil 'packets' considered in this study as 343. This formatted dataset (n = 343) is used for the construction of the Bayesian regression model (BayMBT) and all following exercises.

2.4. Bayesian regression model (BayMBT)

Bayes' theorem (or Bayes' rule) is a method to determine the probability or outcome of an event given some prior knowledge (e.g. a hypothesis) that might be related to the outcome. Bayes' rule in the general form is:

$$p(\text{hypothesis}|\text{data}) = \frac{p(\text{data}|\text{hypothesis})p(\text{hypothesis})}{p(\text{data})} \tag{3}$$

where p(hypothesis|data) is the posterior probability, p (hypothesis) is the prior probability, p(data|hypothesis) is the likelihood, and p(data) is the marginal likelihood.

Following the approach of Tierney and Tingley (2014), who obtained a calibration model to estimate sea surface temperatures based on isoprenoidal GDGTs, Bayes' rule is applied twice here: once to infer regression parameters between MBT'_{5Me} and gridded MAAT, and second to predict MAAT from MBT'_{5Me} values.

The first application of Bayes' rule is used to infer the parameters of a linear regression model of the general form:

$$\mathbf{Y} = \mathbf{X\beta} + \epsilon \tag{4}$$

$$\varepsilon \sim N(0, \sigma^2, \mathbf{I}) \tag{5}$$

where Y is a n × 1 vector of MBT'_{5Me} values, X is a n × 2 matrix of corresponding gridded MAAT (where the second column is a column of ones), β is a 2 × 1 vector of the regression parameters (i.e. slope and intercept) and ϵ is a n × 1 vector of the error, which is normally distributed around zero with a variance of σ^2. By assigning the Y parameter as MBT'_{5Me} and the X parameter as gridded MAAT the relationship between MBT'_{5Me} and gridded MAAT is formulated in the etiologically correct way.

Bayesian inference of the parameters is thus:

$$p(\boldsymbol{\beta}, \sigma^2|\mathbf{Y}) = p(\mathbf{Y}|\boldsymbol{\beta}, \sigma^2) * p(\boldsymbol{\beta}, \sigma^2) \tag{6}$$

where $p(\boldsymbol{\beta},\sigma^2|\mathbf{Y})$ is the posterior probability of the regression parameters β and σ^2 given the values of MBT'_{5Me}, $p(\mathbf{Y}|\boldsymbol{\beta},\sigma^2)$ is the likelihood of the MBT'_{5Me} values given the regression parameters, and $p(\boldsymbol{\beta},\sigma^2)$ is the prior on the regression parameters. The priors on β and σ^2 are conjugate (Multivariate Normal and Inverse Gamma, respectively) and the resulting conditional posteriors are:

$$\boldsymbol{\beta}|\cdot \sim N(\boldsymbol{\Psi}\mathbf{V}, \mathbf{V}) \tag{7}$$

where

$$\boldsymbol{\Psi} = \mu_0\sigma_0^{-2}\mathbf{I} + \mathbf{X}^T\mathbf{Y}\sigma_n^{-2} \tag{8}$$

$$\mathbf{V} = (\sigma_0^{-2}\mathbf{I} + \mathbf{X}^T\mathbf{X}\sigma_n^{-2})^{-1} \tag{9}$$

And

$$\sigma_n^2 \sim IG(a, b) \tag{10}$$

where

$$a : a_\varnothing + \frac{N}{2} \tag{11}$$

$$b : \left(b_\varnothing + \frac{1}{2}\right) * (\mathbf{Y} - \mathbf{X\beta})^T(\mathbf{Y} - \mathbf{X\beta}) \tag{12}$$

μ_0 and σ_0 are priors on **β,** and $a_\varnothing$ and $b_\varnothing$ are priors on σ_n^2. We use a Gibbs sampler to draw from these conditional posterior distributions of β and σ^2 (Gelman, 2003) and generate an ensemble of possible values of the slopes, intercepts, and error variances of the calibration model.

The second application of Bayes' rule, i.e. the step used to invert the relationship between the X and Y variables to estimate MAAT, is the 'prediction model', which takes the form:

$$p(\mathbf{MAAT}|\mathbf{MBT}, \boldsymbol{\beta}, \sigma^2) \propto p(\mathbf{MBT}|\mathbf{MAAT}, \boldsymbol{\beta}, \sigma^2) * p(\mathbf{MAAT}) \tag{13}$$

where $p(\mathbf{MAAT}|\mathbf{MBT},\boldsymbol{\beta},\sigma^2)$, $p(\mathbf{MBT}|\mathbf{MAAT},\boldsymbol{\beta},\sigma^2)$ and p (**MAAT**) are the posterior probability, the likelihood, and the prior, as above.

The full conditional posterior is:

$$\mathbf{MAAT}|\cdot \propto N(\boldsymbol{\Psi}\mathbf{V}, \mathbf{V}) \tag{14}$$

where

$$\boldsymbol{\Psi} = \mu_M\sigma_M^{-2}\mathbf{I} + \boldsymbol{\beta}^T\mathbf{Y}\sigma^{-2} \tag{15}$$

$$\mathbf{V} = (\sigma_M^{-2} + \boldsymbol{\beta}^T\boldsymbol{\beta}\sigma^{-2})^{-1} \tag{16}$$

Inference of MAAT proceeds by plugging in each paired slope, intercept, and error variance value into the conditional posterior such that the uncertainties in the regression parameters are propagated through to the estimation.

The second application of the Bayesian model requires the choice of a prior mean (μ_M) and a prior standard deviation (σ_M) in order to predict MAAT from MBT'_{5Me} values. For the inferences in this work, the prior mean is set to the mean of modern MAAT across all soil locations (10 °C). The prior standard deviation is set to triple the standard deviation across modern MAAT (30 °C). A large standard deviation is chosen to ensure the MAAT predictions are dominated by the MBT'_{5Me}-MAAT regression model (see discussions in Tierney and Tingley, 2014, 2018).

3. RESULTS

3.1. Sample selection

Due to the statistical similarity of the peat-specific calibration (Naafs et al., 2017b) and the soil calibrations (De Jonge et al., 2014b, Naafs et al., 2017a), there is no strong evidence that these datasets should be separated (Fig. 1B; Appendix B). We also find no difference in the Pearson correlation coefficient of the MBT'_{5Me} index with MAAT between the soil and peat dataset (n = 663, r = 0.79) and the soil-only dataset (n = 567, r = 0.79).

Previously, Naafs et al. (2017a) found that excluding soils with a high proportion of 6-methyl brGDGTs (IR > 0.5) improved calibration statistics. However, in our expanded dataset, we find that the Pearson correlation coefficient between MBT'_{5Me} and gridded MAAT only nominally increases if the soils/peats with an IR > 0.5 are removed, going from 0.79 (whole dataset, n = 663) to 0.80 (IR < 0.5, n = 311). Therefore, in the interest of retaining as much data as possible, we included soils with IR > 0.5 in the Bayesian calibration model.

3.2. Bayesian calibration model

The prior and posterior distributions for the slope, intercept and error variance of the Bayesian calibration model based on the MBT'_{5Me} index, i.e. BayMBT, are shown in Fig. 2A. The posterior distributions are greater in probability density and far narrower than the prior distributions, indicating that the likelihood exerts the bulk of control on the posterior, rather than the prior.

The RMSE of predicted temperatures using the BayMBT model is 6.0 °C (Table 2). The upper limit of the BayMBT model is ~30 °C, and the lower limit is ~−26 °C. A comparison of MAAT residuals from the BayMBT model (Fig. 2C) with Fig. 9D of De Jonge et al. (2014b) shows that the leaning trend in MAAT residuals is resolved, as revealed by the low Pearson correlation coefficient (r = 0.08, Fig. 2C). However, the scatter (MAAT residuals ranging from −18 to 22 °C) at sites with MAAT between 0 and 15 °C (i.e. soils residing at mid-latitudes; Fig. 2C) remains a large source of uncertainty in the calibration.

3.3. Alternative calibration models

To test the sensitivity of the BayMBT model for potentially confounding factors, we developed seven sub-models using different subsets of the soil dataset. We explored modified regression models that consider seasonal variation, the timing and length of the growing season, and days without freezing. The effect of a large temperature shift throughout the annual cycle is tested with the BayMBTHighSeas model, which excludes all soils/peats with low temperature seasonality. A cut-off of 20 °C was chosen (see Fig. 3A). Conversely, the BayMBTLowSeas model excludes soils with temperature seasonality > 20 °C. The BayMBTLowSeas model has a R^2 value of 0.76, whereas the R^2 of the BayMBTHighSeas model is 0.13 (Table 2).

The next set of models, i.e. the $BayMBT_0$, $BayMBT_{-5}$, and $BayMBT_{-10}$ models, calibrate the MBT'_{5Me} index to

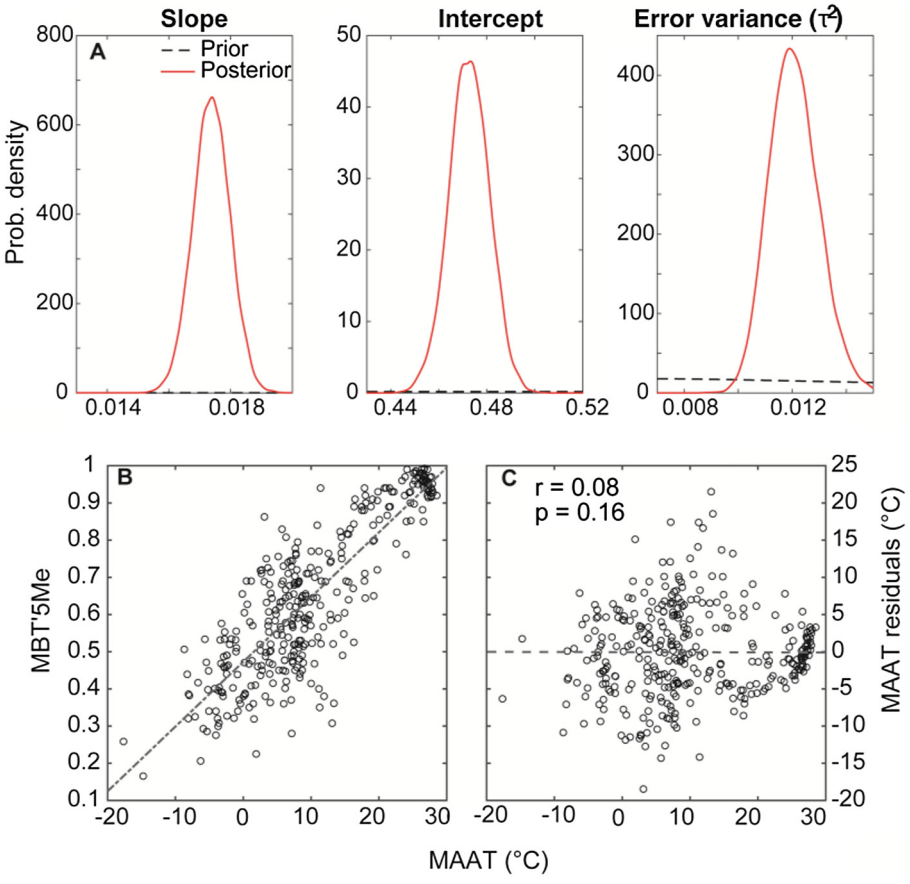

Fig. 2. (A) Plot of prior (dotted black lines) and posterior (solid red lines) probability density functions for the slope, intercept, and error variance of the BayMBT calibration model. (B) Plot of the Bayesian regression model with fitted line (dashed grey line). (C) BayMBT MAAT residuals plotted against gridded MAAT (CRU TS v. 3.24.01 dataset; Harris et al., 2014). The Pearson correlation coefficient and p value are shown. (For interpretation of the references to color in this figure legend, the reader is referred to the web version of this article.)

Table 2
The BayMBT and other Bayesian regression models for predicting MAAT in global soils. Gridded MAAT values are obtained from the CRU TS v. 3.24.01 dataset (Harris et al., 2014).

Model	n	R^2	Variance in residuals (MAAT)	RMSE (°C)	Upper limit ($MBT'_{5Me} = 1$)	Lower limit ($MBT'_{5Me} = 0$)
BayMBT	343	0.64	36.4	6.0	29.9	−25.6
BayMBTLowSeas	168	0.76	21.7	4.6	29.3	−19.2
BayMBTHighSeas	175	0.13	36.6	6.0	26.9	−25.1
$BayMBT_0$	343	0.70	14.2	3.8	27.1	0.9
$BayMBT_{-5}$	343	0.68	18.3	4.3	27.6	−3.5
$BayMBT_{-10}$	343	0.64	24.4	4.9	27.8	−7.7
BayMBT500	229	0.71	26.3	5.1	28.7	−22.9
BayMBT500 + MAT > 0 °C	229	0.74	14.6	3.8	27.5	−13.2

the average temperature of all months that have an average temperature above 0, −5, and −10 °C, respectively. These models are designed to test the effect of the production of brGDGTs in soils in higher latitudes/altitudes, where the production days may be directly related to the days where temperature does not drop below a certain threshold value. This investigation is functionally similar to the growing degree days parameter investigated by Naafs et al. (2017a), which they found to result in a slightly better R^2 value and a reduction in the range of low temperature residuals. Out of the $BayMBT_0$, $BayMBT_{-5}$, and $BayMBT_{-10}$ set of models, the $BayMBT_0$ model had the highest R^2 value (0.70), followed by the $BayMBT_{-5}$ (0.68), and the $BayMBT_{-10}$ (0.64) models (Table 2).

The influence of aridity is tested with the BayMBT500 model, which excludes all soils/peats with MAP values < 500 mm/year, i.e. dry, arid soils. The BayMBT500 model has a higher R^2 value ($R^2 = 0.71$) and a slightly lower RMSE (5.1 °C) than the BayMBT model (Table 2).

4. DISCUSSION

4.1. Comparison of the BayMBT model with previous calibration models

The RMSE of the BayMBT model is higher than that of previous calibrations using OLS and Deming regressions (De Jonge et al., 2014b; Naafs et al., 2017a). This is part because, in contrast with OLS, the uncertainties in the slope and intercept are captured by the Bayesian inference, but it is also likely due to the expanded dataset considered here. The upper limit for the BayMBT model is substantially higher than previous calibrations ($\Delta T \sim 5$ °C; cf. De Jonge et al., 2014b; Naafs et al., 2017b), increasing the range of temperatures that may be predicted (Fig. 2B). This increased upper limit arises from a slightly steeper slope of the expanded soil dataset as well as the elimination of regression dilution. In contrast, the upper limit of the OLS method using the expanded dataset of this study is only 25 °C (not shown), which is likely an artefact of regression dilution. It is also likely that the addition of the Indian soils with MAAT exceeding 26–27 °C contributes to the steeper slope in the Bayesian regression model. The lower limit of the calibration is also brought down substantially ($\Delta T \sim 10$ °C; Table 2) compared to previous calibrations. This is the result of the steeper slope in the Bayesian regression model, and the addition of soils from Siberia, extending the low end of the MBT'_{5Me} range from 0.35 (De Jonge et al., 2014b) to 0.17 (this study).

4.2. Identifying confounding factors on BayMBT model residuals

The extremely large range of MAAT residuals (~40 °C; Fig. 2C) for soils located at mid-latitudes indicates that MAAT alone fails to explain a substantial portion of the MBT'_{5Me} variance. Here, we explore whether other environmental parameters, namely temperature seasonality, soil pH, and the magnitude and timing of precipitation, may explain this scatter, while recognizing that covariance between environmental variables (e.g. pH vs. MAP and MAAT vs. MAP) could hinder the attribution of variance to a single parameter.

4.2.1. Temperature seasonality

Temperature seasonality (temperature of warmest month – temperature of coldest month) explains some of the variance of the BayMBT MAAT residuals ($r = -0.28$; Fig. 3A). BayMBT overestimates temperatures for soils experiencing high temperature seasonality, which is consistent with a bias of the proxy toward summer temperatures. This follows the earlier suggestion that soil bacteria may preferentially produce brGDGTs during the growing season in summer (Weijers et al., 2007a, 2011; Rueda et al., 2009; Peterse et al., 2012; Deng et al., 2016). However, there are indications that microbial biomass synthesis in soils also continues under frozen conditions (Nedwell, 1999; Drotz et al., 2010) and no seasonal variations in brGDGT distributions were observed in mid-latitude soils over the course of a year (Weijers et al., 2011). Thus, these contrasting observations warrant further investigation into the effect of temperature seasonality on brGDGT distributions in soils.

4.2.2. Soil pH

pH is the primary control on the distribution and abundance of microbes in soils (Lauber et al., 2009). Empirical studies suggest that soil pH influences the degree of cyclisation of brGDGTs (expressed in the CBT index; Weijers et al., 2007a) and the relative abundance of 6-methyl brGDGT isomers (De Jonge et al., 2014b; Dang et al., 2016). Although the calibrations using the MBT'_{5Me} index only include 5-methyl brGDGTs, which are not thought

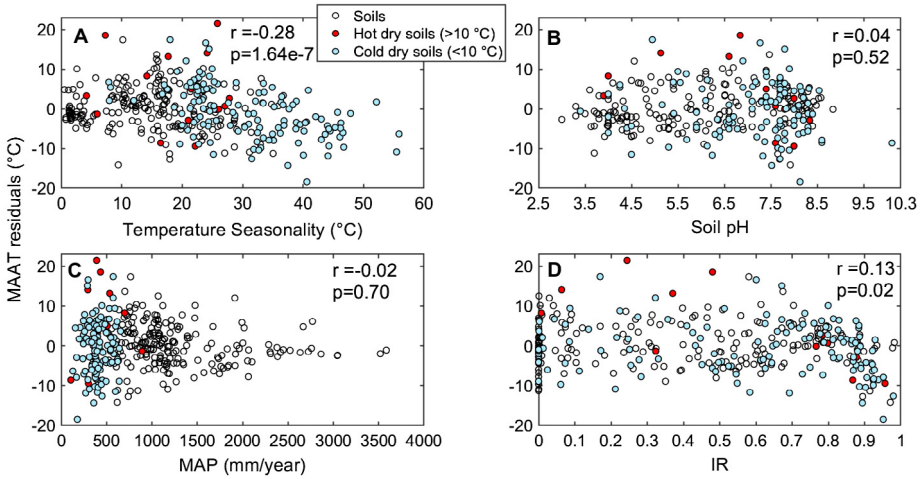

Fig. 3. (A-D) MAAT residuals (gridded – predicted MAT estimates) of BayMBT model plotted against temperature seasonality, Soil pH, MAP, and IR. Arid soils (<600 mm/year) are plotted as blue (<10 °C) and red circles (>10 °C), respectively. (For interpretation of the references to color in this figure legend, the reader is referred to the web version of this article.)

to respond to pH (De Jonge et al., 2014b), a pH effect may not be unexpected, and may have a bearing on the MAAT residuals of the BayMBT model. Overall, the BayMBT model performs slightly better on acidic soils (pH < 6) than alkaline soils (pH > 6), as seen by the larger variance of residuals for alkaline soils compared to acidic soils (i.e. 37.9 vs. 27.7; Fig. 3B; $p = 0.04$). It is also apparent from Fig. 3B-C that alkaline soils with MAAT < 10 °C and a low precipitation (<600 mm/year) are particularly difficult for the BayMBT model to predict, indicated by a larger population variance in low precipitation and alkaline soils than in high precipitation and acidic soils (F-test, $p = 1.1 \times 10^{-3}$). Coincidentally, those soils are located in areas which (i) are located at high altitudes (average ca. 1400 m), and (ii) occur at mid-to-high latitudes in the Northern Hemisphere (31–78 °N). 67% of these alkaline soils with MAAT < 10 °C are located in China. These Chinese soils are further associated with a high temperature seasonality (>25 °C), and a grassland biome. Therefore, while pH may be a meaningful factor dictating the scatter of MAAT residuals, co-variance with other environmental variables makes the prediction of the scatter unclear. As most of the alkaline soils were associated with high temperature seasonality, it is probable that temperature seasonality has a stronger effect than pH on the large scatter of MAAT residuals.

Interestingly, low soil pH is known to reduce bacterial diversity in soils (Lauber et al., 2009), and thus, perhaps on the brGDGT distribution of soil bacteria and their response to environmental parameters. This reduced microbial diversity may explain why the acidic soils perform better in the BayMBT model (Fig. 3B). However, a more detailed discussion on this point is hampered due to missing information on the full identity of microbial brGDGT producers, the response of brGDGT distributions in these bacteria to environmental parameters, and the distribution of these bacteria in soils in different settings.

A trend in MAAT residuals seems apparent at IR values > 0.8, with almost all MAAT residuals having negative values (Fig. 3D). In principle, the abundance of 6-methyl brGDGTs in soils should not have an effect on the MBT'_{5Me} index. However, the non-random behavior in the MAAT residuals at IR > 0.8 suggest some effect, perhaps related to the dominance of bacteria that produce 6-methyl brGDGTs that may also produce small quantities of 5-methyl brGDGTs in these soils.

4.2.3. MAP

The amount and intensity of rainfall can, to some extent, (indirectly) influence the 'wetness' of a soil. Further to that, the soil pH, and by extension brGDGT distributions, are also indirectly influenced by precipitation. Interestingly, the relationship of MAP to the MAAT residuals in Fig. 3C does not possess a significant Pearson correlation coefficient ($r = 0.02$). However, this may be an artefact of the significant correlation between MAAT and MAP throughout the dataset ($r = 0.65$; $p < 0.0001$). Previous studies have shown that MAAT is severely underestimated (>20 °C) in soils at high elevation and in environments with low (<500 mm/year) precipitation (Peterse et al., 2012; Dirghangi et al., 2013; Menges et al., 2014; De Jonge et al., 2014b). However, MAAT residuals of dry soils cluster almost symmetrically around 0 °C in the BayMBT model (Figs. 3C and 4A). The symmetrical distribution is also a result of treating the MBT'_{5Me} index as the dependent variable in the regression. However, the largest spread of MAAT residuals in Fig. 3C is indeed associated with dry soils (MAP < 600 mm/year; $p = 1.8e10^{-4}$ for F-test vs. wet soils > 600 mm/year), suggesting that MAP bears a notable influence on MAAT residuals. The highest residuals for the dry soils are associated with higher gridded MAATs (red circles, Fig. 3C), however the low number of these specific soils ($n = 15$) precludes any statistical tests to determine if this is meaningful.

The distribution of rainfall throughout the year is another factor that could influence the communities of brGDGT-producing soil bacteria, and thus the brGDGT distribution of a soil. For instance, a short duration of precipitation may lead to seasonally arid conditions, therefore

exerting moisture stress on soil microbes. Furthermore, the timing of precipitation in relation to that of the warmer months and growing season could also influence brGDGT production, and hence, distributions. Using the monthly MAP data, the difference in MAP between the month with the maximum amount of rainfall and the overall average amount of rainfall throughout the year was calculated and used to estimate the seasonality of precipitation ($SoP = MAP_{max}$-$\overline{MAP}$). Thus, a low SoP is indicative of a region/soil with an overall low MAP throughout the year, or a region where MAP is constant throughout the year. On the other hand, a high SoP may indicate that rainfall may be concentrated in one time of the year, such as regions that have a heavily distinct 'wet' and 'dry' season. Ergo, the SoP index can aid in interpreting whether a potential production bias is present for regions experiencing various timings of precipitation.

We do not observe a strong correlation between SoP and the residuals; however soils in regions with relatively low SoPs (<100) have a substantially larger scatter in MAAT residuals associated with the model (Fig. 4C), and the variance of the residuals is correlated with SoP ($r = -0.24$, $p = 1.02e\text{-}4$), however slightly less so with MAP (<600 mm/year; $r = 0.15$, $p = 0.07$). In general, soils with a MAAT > 20 °C associated with high SoPs (>100) perform better, with MAAT residuals within a 5 °C range (typical RMSE of the proxy; Figs. 2C and 4C). This indicates that warm soils located in regions with a seasonally heavy rainfall have brGDGT distributions which estimate MAAT relatively well. However, these soils are associated with a lower range of temperature seasonality, which probably leads to a more accurate reconstructed MAAT due to no temperature bias toward a particular season.

4.2.4. Saturation of the BayMBT model at high temperature

A subtle feature of the soils from locations associated with MAAT > 20 °C is that they appear to contain some evidence of non-random distribution in their MAAT residuals (Fig. 2C). This becomes more evident when the MAAT residuals of these soils are plotted against MAAT, temperature seasonality, MAP, altitude, soil pH, and IR (Fig. 5). Several other cutoffs (25 and 15 °C; not shown) were also considered, but 20 °C is the cutoff that consists of a reasonable number of soils ($n = 88$) and shows the most distinctive trend in MAAT residuals. This subset of the data shows clear relationships between MAAT residuals and MAAT ($r = 0.43$), temperature seasonality ($r = 0.36$), soil pH ($r = 0.60$), MAP ($r = -0.47$) and IR ($r = 0.21$). No clear relationship with altitude ($r = -0.17$) was observed for these soils (as is the case for the whole dataset, $r = 0.15$).

The trends in Fig. 5 may indicate that above 20 °C, the MBT'_{5Me} signal represents a complex interplay between the magnitude and timing of precipitation, and temperature seasonality. In particular, BayMBT overestimates MAAT (on average 1.6 ± 0.3 °C) for warm soils linked with high MAP (>2000 mm/year, e.g. tropical rainforests; Fig. 5D). Alternatively, the trends in residuals in Fig. 5 may indicate that the proxy becomes non-linearly sensitive to MAAT as it approaches its saturation point. This raises the question as to whether an adjustment of the MBT'_{5Me} index to deal with non-linearity is needed at this higher end of the calibration, or indeed whether a nonlinear calibration is necessary. However, soil data from India dominate the warm end of the calibration dataset; other warm locations are underrepresented. Thus, fitting a non-linear function at this time might unduly bias a global regression towards Indian soils. A further consideration is that the absolute saturation temperature for this proxy is not explicitly known, given that brGDGT-producing bacteria have not been cultured. It is therefore important to note that the upper limit proposed in this study, 29 °C, may therefore not be a true limit insofar as the bacteria responsible for synthesizing brGDGTs may continue to do so at higher temperatures. Another likely option is the saturation effect could be a result of the fact that brGDGT-synthesizing bacteria only produce

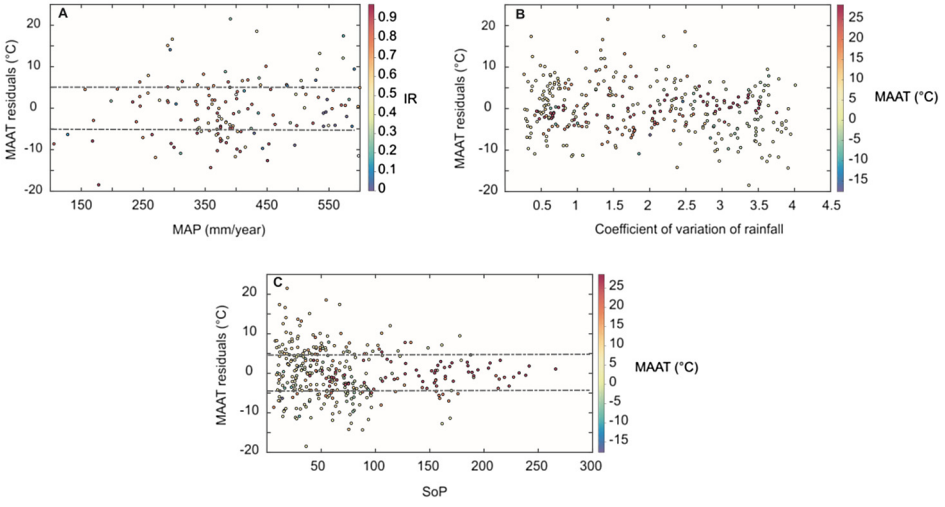

Fig. 4. (A) MAAT residuals (gridded – predicted MAAT estimates) of dry (MAP < 600 mm/year) soils plotted against MAP with circle color fill indicating IR value. (B) MAAT residuals plotted against the coefficient of variation of rainfall (MAP), with circle color fill indicating MAAT. (C) MAAT residuals plotted against the seasonality of precipitation (SoP) index, with circle color fill indicating MAAT. (For interpretation of the references to color in this figure legend, the reader is referred to the web version of this article.)

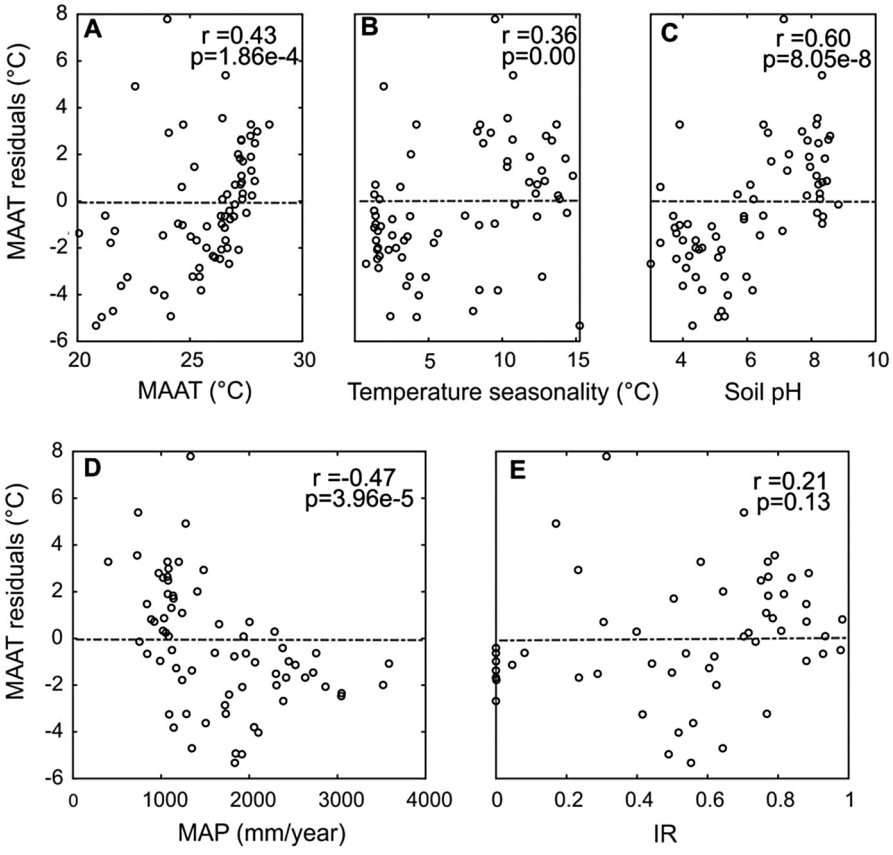

Fig. 5. (A-E) Crossplots of MAAT residuals (gridded – predicted MAAT estimates) of the BayMBT model of soils from settings with a MAAT > 20 °C with (A) MAAT, (B) temperature seasonality, (C) Soil pH, (D) MAP, and (E) IR. Pearson correlation coefficients and p values are plotted.

one type of brGDGT (e.g. tetramethylated brGDGTs) above a certain threshold temperature. However, both options are possible and must be considered as long as the brGDGT-producing bacteria remain unknown and uncultured.

4.3. Assessing the influence of confounding factors on the BayMBT model performance

4.3.1. Influence of temperature seasonality

The low R^2 of the BayMBTHighSeas model is most likely an artefact of the exclusion of the high-MAAT soils that anchor the calibration at the higher MAAT (>25 °C) end of the calibration. Nevertheless, it is important to note the tighter fit of the BayMBTLowSeas model compared to the BayMBT model (Table 2). It seems that seasonal biases in MAAT estimates are more pronounced in soils where temperature seasonality exceeds 20 °C, regardless of location or latitude (Fig. 3A). Soils with large temperature seasonality (n = 175) occur in both mid to high latitudes (Fig. 6), although there are only 15 soils with temperature seasonality > 20 °C located in 'high' latitudes areas (>60° N, in Finland, Russia, Sweden, Canada, USA, Iceland, and Svalbard). Both the BayMBTHighSeas and BayMBTLowSeas models are associated with a high RMSE (6.0 and 4.6 °C, respectively), and contain a large degree of scatter in the proxy that affects the accuracy of predicted MAAT. Despite the improved regression parameters of the BayMBTLowSeas model, the smaller sample size and exclusion of a large proportion of soils (~50%) does preclude its adoption as a calibration to reconstruct paleoclimate.

Calibration of MBT'_{5Me} to gridded temperatures of the warmer months, shows that the $BayMBT_0$ and $BayMBT_{-5}$ models possess the most improved RMSE values (3.8–4.3 °C) compared to the BayMBT. However, the coefficient of

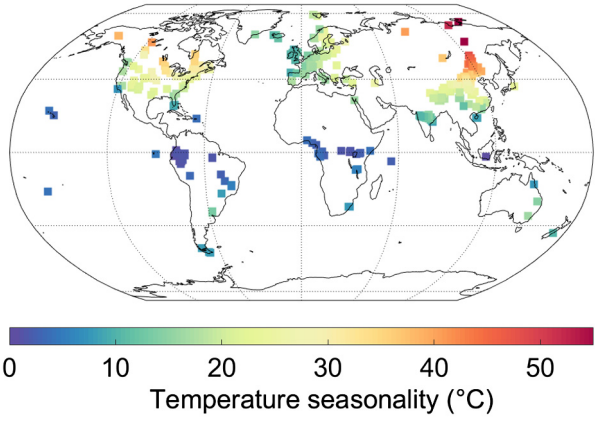

Fig. 6. Global map showing soils plotted with corresponding values for temperature seasonality (obtained from CRU TS v. 3.24.01; Harris et al., 2014).

determination value (R^2) for the $BayMBT_0$ is only marginally higher than that of the BayMBT model (Table 2, Fig. 7). The $BayMBT_{-5}$ and $BayMBT_{-10}$ models do not exhibit any advantage over the $BayMBT_0$, however, the $BayMBT_{-5}$ model still performs better than the BayMBT and BayMBTHighSeas models in terms of R^2 and RMSE values.

The lower RMSE of the threshold-based $BayMBT_0$ suggest that calibration to temperatures above the freezing point of water (0 °C) may more accurately describe variation in MBT'_{5Me}. Indeed, a study that examined the seasonal variation of bacterial communities in the active layer of permafrost from Svalbard demonstrated that the strongest changes in community structure recorded by DNA and RNA-based analyses occurred during the freezing in October and the spring thaw in May (Schostag et al., 2015). This raises the question of whether brGDGT-producing microbes are part of distinct communities that are more abundant in the summer as opposed to the winter. Indeed, a recent study that paired microbial community composition with brGDGT lipid distributions in geothermally heated soils determined that bacterial community changes from colder to warmer soils are associated with variability in the MBT'_{5Me} index (De Jonge et al., 2019). However, this interpretation remains speculative until brGDGT production has been demonstrated in other bacterial phyla.

The fact that the $BayMBT_0$ model is inclusive of all soils considered, together with the lower RMSE (3.8 °C) and lowest variance of MAAT residuals indicates that it is the most suitable calibration to apply to paleoclimate datasets. Besides, the $BayMBT_0$ model also takes the strong effect of temperature seasonality and potential seasonality of brGDGT production on the calibration models into account. However, if $BayMBT_0$ is used for paleoclimate reconstruction, one must be aware of the difference in temperatures (i.e. all months above zero vs. annual average temperatures) reconstructed by the BayMBT and $BayMBT_0$ calibrations, respectively.

4.3.2. Influence of precipitation amount and seasonality

The slight improvement of the BayMBT500 model may arise from the reduced size of the dataset (Table 2). The BayMBT model does not structurally underestimate MAAT in arid regions (Fig. 3C), as was the case in the calibration of Peterse et al. (2012). The removal of the temperature bias in arid soils is a result of the removal of the 6-methyl brGDGTs from the MBT'_{5Me} index, and was already observed in the calibration of De Jonge et al. (2014b). Due to the decreased size of the dataset, we find little justification for adopting BayMBT500.

The BayMBTIR model has similar values for the coefficient of determination ($R^2 = 0.64$) and RMSE (5.9 °C, Table 2) to the original BayMBT model. Removing the soils with IR > 0.8 does not substantially improve the prediction of MAAT for global soils. Thus, the BayMBTIR model in this study suggests that an increased proportion of 6-methyl brGDGTs in soils does not appear to have a substantial impact on proxy calibration based on 5-methyl brGDGTs discussed here.

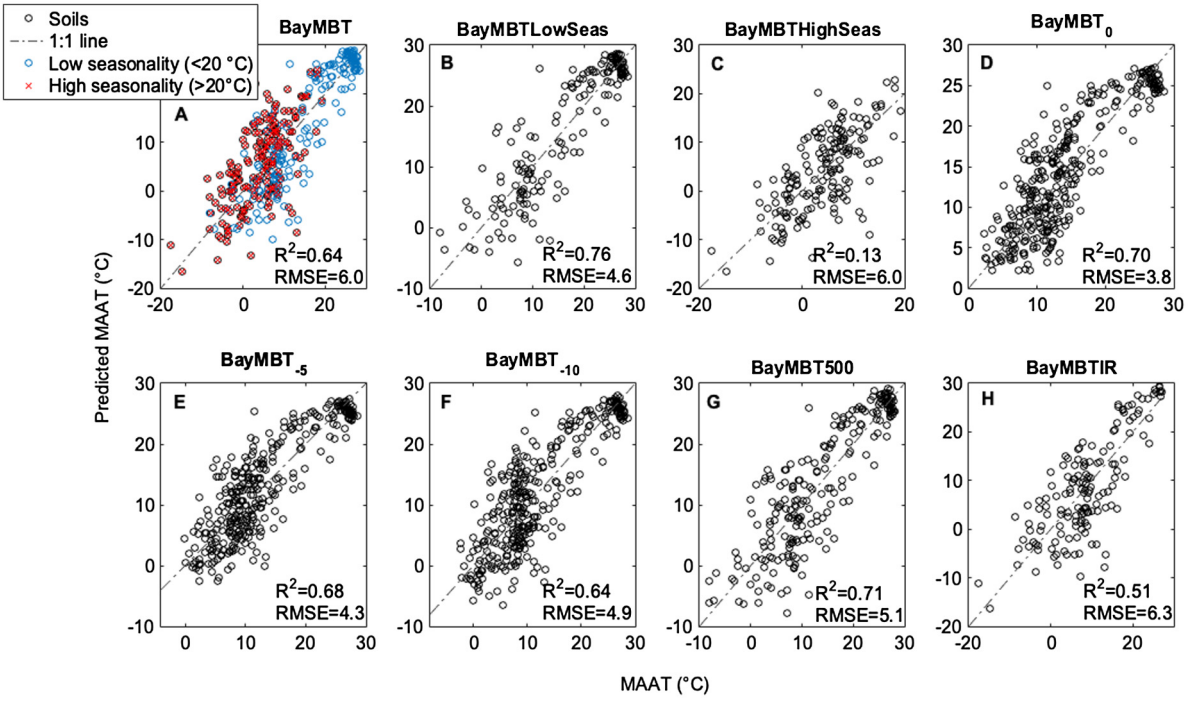

Fig 7. Plots of gridded MAAT vs. predicted MAAT for the eight Bayesian regression models. (A) the BayMBT model, with high (>20 °C, red cross) and low (<20, blue circle) temperature seasonalities represented by red crosses and blue circles, respectively. (B) the BayMBTLowSeas, (C) BayMBTHighSeas, (D) $BayMBT_0$, (E) $BayMBT_{-5}$, (F) $BayMBT_{-10}$, (G) BayMBT500, and (H) BayMBTIR models, respectively. A 1:1 reference line has been added to each plot and the coefficients of determination (R^2) and RMSE values are shown. (For interpretation of the references to color in this figure legend, the reader is referred to the web version of this article.)

4.4. Reasons for the remaining scatter in the BayMBT model

Despite the better performance of the $BayMBT_0$ model, which reduces part of the scatter at mid-latitudes, the source of the persistent remaining scatter remains elusive. The first source of the scatter discussed here is the choice of method used for the MAAT estimates in the calibration (Section 2.3). For example, the 0.5° gridded CRU TS v. 3.24.01 (Harris et al., 2014) dataset may not be highly resolved enough to estimate temperature for regions with micro-topography. This may lead to large differences in the gridded MAATs with actual temperatures at a specific location. However, the absence of residual patterns that trend with altitude ($r = 0.15$; $p = 0.03$; not shown), indicate that this factor does not exert a strong influence on the calibration.

Another possible source of the scatter at mid-latitudes is the potential offset between soil and air temperature (Weijers et al., 2011). This offset is not equal everywhere, and could account for a large proportion of residual scatter in Figs. 2C and 3. For example, Grundstein et al. (2005) found that the annual thermal offset with MAAT for soils from North Dakota experiencing a seasonal snow cover ranged between 1.5 and 4 °C, over the study period 1990–2001. For the soils in this study that experience snow cover, the influence of snowpack insulation on the offset between soil/air temperatures could play a significant role on predicted temperatures using the BayMBT model. The offset between soil and air temperature may be caused by the presence of soils in the dataset which are located in areas that are perennially shaded, affected by vegetation, or by virtue of being located on the northern side of a mountain, for example. Unfortunately, soil temperature data is not available for the soils included in this study, which precludes any further investigation into this effect.

A third source for the large scatter at mid-latitudes could relate to the microbial community composition in soils, which may be different in cold and warm, or high and low temperature seasonality soils (Delgado-Baquerizo et al., 2016, 2017). Since only a very limited portion of the microbial population in soils are known to produce brGDGTs, this influence on the scatter of the residuals of the BayMBT model is hard to elucidate. Nevertheless, different brGDGT-producing communities could have distinct relations to temperature (Oliverio et al., 2017). BrGDGTs have only presently been identified in 2 out of 46 strains of *Acidobacteria* (Sinninghe Damsté et al., 2018), and most of the brGDGT structures are still 'orphans'. A recent study by Oliverio et al. (2017) compared the temperature response of soil microbes and found that the relative abundance of most (13 out of 15) phylotypes within the family *Koribacteraceae* in *Acidobacteria* decreased as temperature increases. This observation was found to hold true for other families (*Acidobacteriaceae* and *Soilbacteres*) within the *Acidobacteria* phylum, as well as some families within the *Proteobacteria* phylum, which are the two most dominant soil phyla in the Northern Hemisphere (Oliverio et al., 2017). Hence, it is possible that temperature-dependent changes in the relative abundances of brGDGT producers with distinct MBT'_{5Me}-MAAT relationships may contribute to the high scatter in this proxy. However, the empirical observation that the degree of branching of brGDGTs in the membrane of microbes changes with temperature is likely a physical adaptation that probably does not vary too much from species to species.

Interestingly, 98% (172/175) of soils in the BayMBTHighSeas model reside in mid-latitudes, compared to only 32 % (53/168) of soils in the BayMBTLowSeas model. Due to the higher R^2 value of the BayMBTLowSeas model compared to the BayMBTHighSeas model (Table 2), the source of the scatter in the latter could be a result of a microbial community shift or the co-occurrence of multiple communities that respond differently to temperature change. The diversity of brGDGT-producing bacteria in the mid-latitude soils with distinct relationships to temperature may thus lead to scatter in the calibration. If the brGDGT-producers were eventually identified, this raises an important question: is it possible to know which community dominates when? However, as mentioned before, the difference in R^2 values between the BayMBTLowSeas and BayMBTHighSeas models may be a result of the exclusion of soils associated with high MAATs in the BayMBTHighSeas model, so this question cannot be immediately answered. Future work that combines DNA studies with lipid brGDGT abundances in soils along a latitudinal and/or seasonality gradient would be a step forward in understanding and answering this question.

5. BAYMBT PALEOCLIMATE APPLICATION

In this section we test the performance of the $BayMBT_0$ model on brGDGTs in an Eocene lignite sequence from Western Europe (Inglis et al., 2017), as well as on brGDGTs in Pliocene sediments from the North Sea Basin, after correction for a possible in situ marine overprint (Dearing Crampton-Flood et al., 2018). We compare and contrast the reconstructed temperatures of these two records, termed $MAAT_0$ (the mean temperature of all months > 0 °C) with MAAT obtained using the soil (De Jonge et al., 2014b; Naafs et al., 2017a) and peat (Naafs et al., 2017b) calibrations.

5.1. Eocene climate in Western Europe

The BayMBT models have a higher upper limit (i.e. 27 °C for $BayMBT_0$) compared to that of previous calibrations, which should make them better suited to reconstruct the higher temperatures during greenhouse periods of Earth's history, such as the Eocene. To illustrate, a recent study that used brGDGTs in a lignite sequence from western Europe to reconstruct paleotemperatures for the Eocene concluded that the magnitude for early Eocene warming (2–3 °C) was likely a minimum estimate, as reconstructed temperatures reached up to 26 °C, 1–2 °C higher than the upper limit of the De Jonge et al. (2014b) calibration used (Inglis et al., 2017). In contrast, temperature reconstructions for the Bighorn Basin, Wyoming based on leaf physiognomy indicate that the amplitude of early Eocene warming was much larger, in the order of 4–6 °C (Wilf, 2000). This is also corroborated by TEX_{86} sea surface temperature (SST) reconstructions, which also show a

warming of 4–6 °C for the same time interval in both the Western Siberian Sea (Frieling et al., 2014), and the South West Pacific (Hollis et al., 2012; Bijl et al., 2013; Inglis et al., 2015). We test here if the application of the BayMBT$_0$ model to the lignite record will result in a larger amount of warming than initially reconstructed. Due to the deep-time application, modern MAAT could not be used to estimate the prior mean. Instead, an average of the MAT$_{mr}$ temperatures presented in Inglis et al. (2017) was chosen (24 °C) as the prior mean. A suitably broad prior standard deviation of 15 was chosen, in order to avoid placing too much emphasis on the prior mean. An effect of a smaller and larger choice of prior standard deviation on the model outcomes is discussed in Tierney and Tingley (2014). In brief, unless the prior standard deviation is set to be unrealistically small (e.g., less than 5 °C), the choice of prior standard deviation does not exert much bearing on the MAAT predictions.

The absolute MAAT$_0$ reconstructed using BayMBT$_0$ for the Eocene lignites ranges between 25 and 27 °C (Fig. 8). These temperatures are ~2 °C warmer than temperatures using MAT$_{mr}$, and ~4 °C warmer than temperatures reconstructed using MBT′$_{5Me}$ (De Jonge et al., 2014b). The warmer temperatures reconstructed using BayMBT$_0$ are likely a result of the reconstruction of temperatures of all months > 0 °C, which produces warmer temperatures. Despite the difference in reconstructed temperatures (MAAT$_0$ vs. MAAT), the BayMBT$_0$ model yields a similar estimate for the magnitude of early Eocene warming (~2 °C) as the original MAT$_{mr}$ and MBT′$_{5Me}$-based (De Jonge et al., 2014b) temperature records (main seam to seam 3; Fig. 8; Inglis et al., 2017). However, caution should be used when comparing these warming estimates as MAAT and MAAT$_0$ are not equivalent.

Importantly, the upper limit of the BayMBT$_0$ is reached, so the magnitude of early Eocene warming using this calibration may still be underestimated. In contrast, the magnitude of warming using the peat calibration (Naafs et al., 2017b) is slightly higher, at 4 °C. The average early Eocene temperature of ~27 °C (Seams 3–9) predicted using BayMBT$_0$ is 4–5 °C higher than MBT′$_{5Me}$ estimates using the De Jonge et al. (2014b) calibration, but 1–2 °C lower than the Naafs et al. (2017b) peat calibration (Fig. 8). However, as long as the calibration used is based on the MBT′$_{5Me}$ index, the saturation state will not change and the maximum temperature will depend on the temperature limit of the model. Regardless, the absolute reconstructed MAAT$_0$ temperatures using the BayMBT$_0$ model and the MAAT using the peat calibration (Naafs et al., 2017b) better fit with TEX$_{86}$-based early Eocene sea surface temperature reconstructions, indicating that also continental temperatures were above 25 °C at mid- and high latitudes (Frieling et al., 2014).

5.2. Pliocene climate of Northwestern Europe

A recent terrestrial temperature reconstruction of the Pliocene Northwestern Europe indicated that temperatures during the Early-Mid Pliocene were mostly stable, and fluctuated between 10–13 °C (Dearing Crampton-Flood et al., 2018). A decrease in temperatures of ~3 °C is visible in the younger part of the record, and corresponds to the Plio-Pleistocene transition. Absolute temperatures in the corrected record of Dearing Crampton-Flood et al. (2018) were comparable with temperatures reconstructed from pollen assemblages in Northwestern Europe (13–14 °C; Head, 1998; Uhl et al., 2007; Utescher et al., 2000). Thus, application of the BayMBT$_0$ model may further reduce the error associated with this record, and further constrain the temperature estimates for the Pliocene of NW Europe. The published temperature record of Dearing Crampton-Flood et al. (2018) has been corrected for possible marine overprint by 'subtracting' the marine MBT′$_{5Me}$ value from the total 'mixed' MBT′$_{5Me}$ values in the sediments. We use the corrected MBT′$_{5Me}$ indices, representing the terrestrial component, as input for the BayMBT$_0$ model. A prior mean of 10 °C (modern MAAT of the Netherlands) and a prior standard deviation of 15 were chosen as model input.

The trends in the records generated by all three methods are practically identical (Fig. 9). As expected due to the difference in reconstructed temperatures of the calibrations, the MAAT$_0$s reconstructed using BayMBT$_0$ are higher than

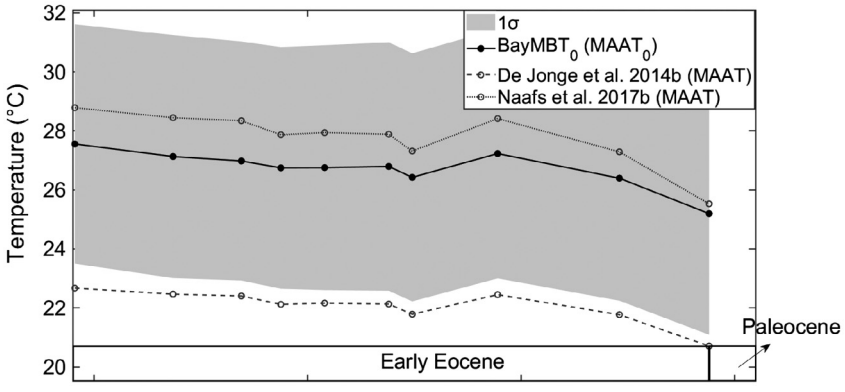

Fig. 8. Reconstructed continental temperatures during the Eocene from a series of lignites (black circles) located in the Schöningen Südfeld mine in Germany (Inglis et al., 2017). Lignite seams (thickness not to scale) and approximate ages are indicated. MAAT reconstructed using the MBT′$_{5Me}$ based MAT estimates using the Naafs et al. (2017b; dotted lines), and De Jonge et al. (2014b; dashed lines) calibrations. The MAAT$_0$ record reconstructed using the BayMBT$_0$ calibration is depicted by a solid lines. The shaded region indicates the 1σ error on the BayMBT$_0$ record.

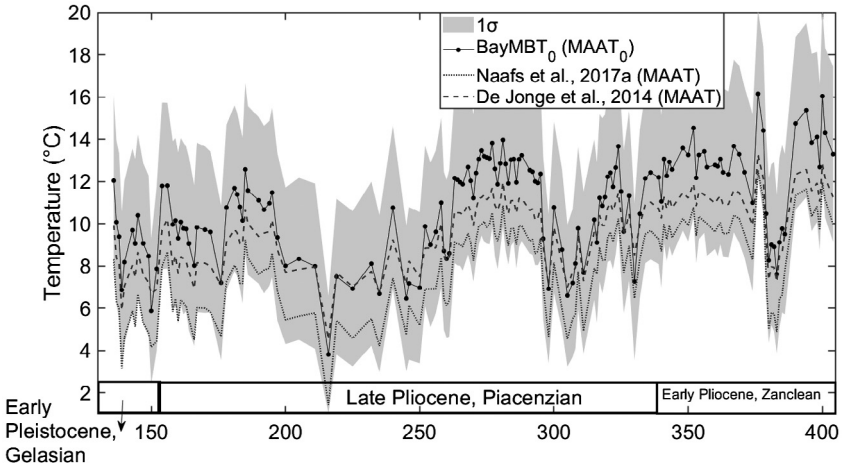

Fig. 9. Reconstructed temperatures for the Pliocene marine sediment sequence from the Hank core located in the Netherlands (Dearing Crampton-Flood et al., 2018). The $BayMBT_0$ (solid line with black circles), De Jonge et al. (dashed line; 2014b), and Naafs et al. (dotted line; 2017a) calibrations based on a corrected MBT'_{5Me} index are plotted against depth and relative ages. The shaded region indicates the 1σ error on the $BayMBT_0$ record.

those of the De Jonge et al. (2014b) and Naafs et al. (2017a) soil calibrations, by 1–3 and 3–4°, respectively. However, the pollen assemblage of warm-adapted species (e.g. *Taxodium*) found in sediments from the Netherlands indicate that it is unlikely that temperatures went below zero for extended amounts of time during the Pliocene (Zagwijn, 1963; Suc and Zagwijn, 1983; Pross and Klotz, 2002). This provides more confidence in comparing the temperatures reconstructed using the De Jonge et al. (2014b) and Naafs et al. (2017a) calibrations (i.e. MAAT) with the $MAAT_0$ reconstructed using the $BayMBT_0$ calibration. All records show a decrease in temperature from the early Pliocene to the Pleistocene/late Pliocene, reflecting the global climate cooling that took place that the end of the Pliocene (Fig. 9).

The slightly higher absolute $BayMBT_0$-derived temperatures for the Early and Late Pliocene (~13–16 °C) fit well with reconstructed temperatures based on pollen from Germany (13.9 ± 0.5 °C; Uhl et al., 2007), England (12.8 ± 1.3 °C; Head, 1998) and the Lower Rhine Basin (14.1 ± 0.2 °C; Utescher et al., 2000). Moreover, $MAAT_0$ estimates from the $BayMBT_0$ model actually better agree with temperature estimates for the mid-Pliocene in Germany (13.8 ± 0.4 °C) based on the HadAM3 GCM model (Pope et al., 2000; Haywood et al., 2002; Salzmann et al., 2008), compared to the original calibration of De Jonge et al. (2014b). $MAAT_0$ estimates from the $BayMBT_0$ record are also associated with a smaller error (3.8 °C; Table 2) than the original record, therefore increasing the reliability of the Pliocene temperature record for inclusion into climate models.

6. CONCLUSIONS

Our study presents the BayMBT model that utilizes Bayes' rule to calibrate the relationship between MBT'_{5Me} and MAAT. The BayMBT model encompasses an expanded dataset that includes both soils and peats, and improves the coverage of the Asian continent. In this new model, the regression dilution of previous calibrations is removed, allowing for a more detailed investigation of the effects of confounding factors on the MBT'_{5Me} for soils. The largest MAAT residuals of the BayMBT model belong to mid-latitude soils with a high temperature seasonality (>20 °C). The large scatter may speculatively be attributed to several co-existing communities of brGDGT-producing soil bacteria. A series of modified calibrations indicates that the most accurate temperature reconstructions can be obtained using the $BayMBT_0$ model. This model is based on the mean temperature of all months above 0 °C, which produces a record of $MAAT_0$, which must be taken into account when interpreting paleotemperature reconstructions using this model. Finally, we stress the need for studies measuring both DNA and lipids to make a step forward in constraining the temperature control on brGDGT-producing microbial communities and resolving the large scatter of MAAT residuals at mid-latitudes.

RESEARCH DATA AND MATLAB CODE

The MATLAB code for the BayMBT and $BayMBT_0$ models are available on the GITHUB repository of J.E.T (https://github.com/jesstierney). The soil dataset used in this study is available on Pangaea.

ACKNOWLEDGEMENTS

The work was supported by funding from the Netherlands Earth System Science Center (NESSC) through a gravitation grant (NWO 024.002.001) from the Dutch Ministry for Education, Culture and Science to JSSD and co-PIs. JET was supported by National Science Foundation grant EAR-1603674. FP acknowledges funding from ETH Fellowship FEL-36 11-1 (New Zealand soil), NWO Veni grant 863.13.016 (Indian soils), and KNAW China Exchange Program grant 530-6CDP17 (Chinese soils). We would like to thank Sebastian Breitenbach (Ruhr-University Bochum) for soil collection in Siberia. Thanks to Tian Ma and Jingjing Guo (Institute of Botany, Chinese Academy of Sciences) for help with extractions of the Chinese soils. We would also like to thank the associate editor and the contribution of three anonymous reviewers whose comments greatly improved the manuscript.

APPENDIX A

See Fig. A1.

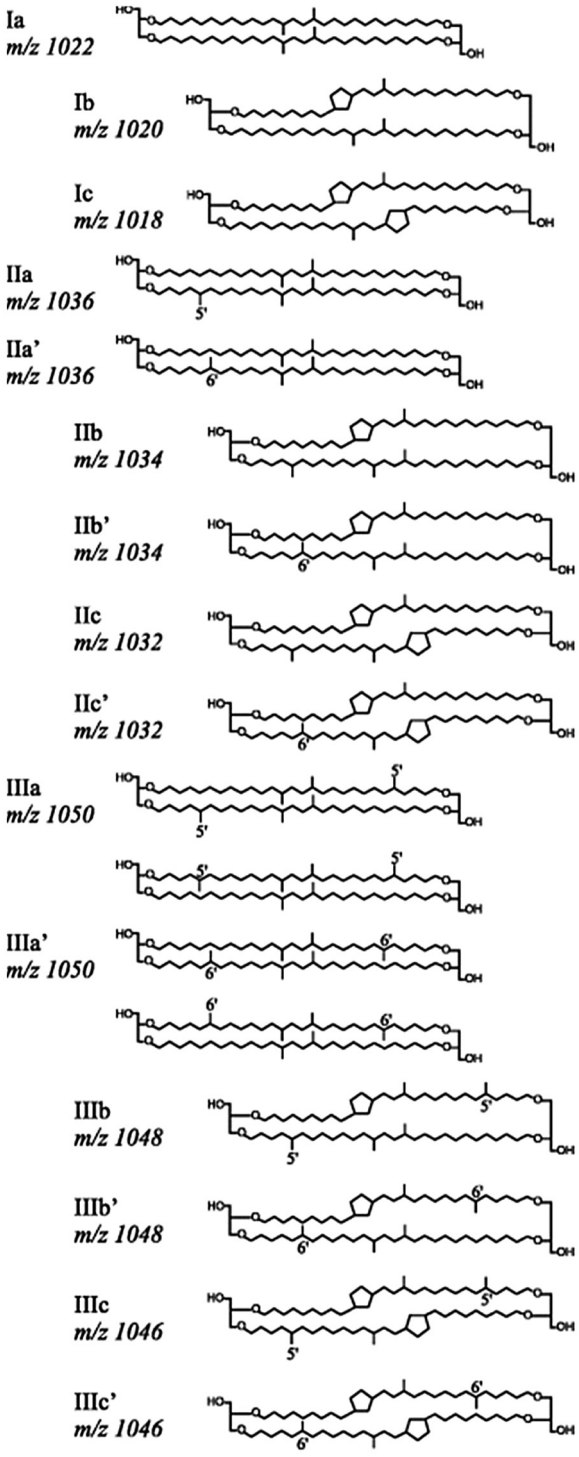

Fig. A1. Molecular structures of the tetramethylated (Ia-Ic), pentamethylated (IIa-IIc), and hexamethylated (IIIa-IIIc) brGDGTs. Isomers of the penta- and hexamethylated brGDGTs are denoted by a methyl group present on the C-5 or C-6' position. From De Jonge et al. (2014b).

APPENDIX B

See Fig. B1.

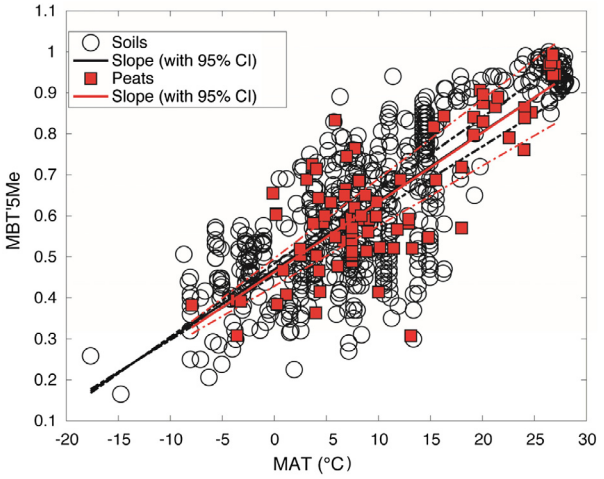

Fig. B1. Statistical similarity of the Peat (Naafs et al., 2017b) and soil calibrations.

APPENDIX C

See Fig. C1.

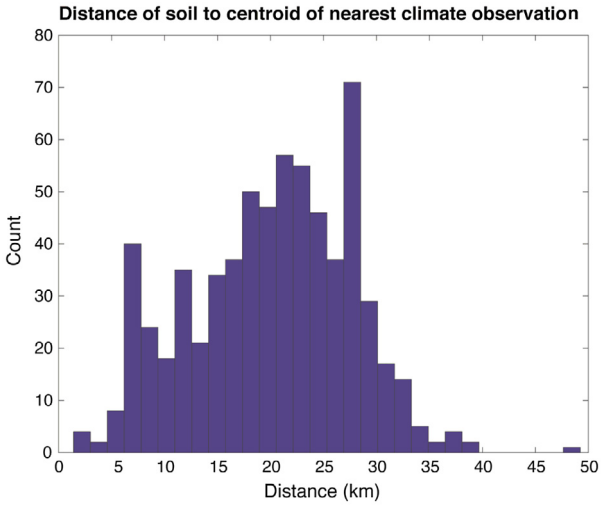

Fig. C1. Histogram of chordal distances between soil locations and gridboxes from CRU MAAT dataset (Harris et al., 2014).

REFERENCES

Ballantyne A. P., Greenwood D. R., Sinninghe Damsté J. S., Csank A. Z., Eberle J. J. and Rybczynski N. (2010) Significantly warmer Arctic surface temperatures during the Pliocene indicated by multiple independent proxies. *Geology* **38**(7), 603–606.

Bijl P. K., Bendle J. A., Bohaty S. M., Pross J., Schouten S., Tauxe L., Stickley C. E., McKay R. M., Röhl U., Olney M. and Sluijs A. (2013) Eocene cooling linked to early flow across the Tasmanian Gateway. *P. Natl. Acad. Sci.* **110**(24), 9645–9650.

Chen Y., Zheng F., Chen S., Liu H., Phelps T. J. and Zhang C. (2018) Branched GDGT production at elevated temperatures in anaerobic soil microcosm incubations. *Org. Geochem.* **117**, 12–21.

Dang X., Yang H., Naafs B. D. A., Pancost R. D. and Xie S. (2016) Evidence of moisture control on the methylation of branched glycerol dialkyl glycerol tetraethers in semi-arid and arid soils. *Geochim. Cosmocim. Acta* **189**, 24–36.

De Jonge C., Hopmans E. C., Stadnitskaia A., Rijpstra W. I. C., Hofland R., Tegelaar E. and Sinninghe Damsté J. S. (2013) Identification of novel penta-and hexamethylated branched glycerol dialkyl glycerol tetraethers in peat using HPLC–MS 2, GC–MS and GC–SMB-MS. *Org. Geochem.* **54**, 78–82.

De Jonge C., Stadnitskaia A., Hopmans E. C., Cherkashov G., Fedotov A. and Sinninghe Damsté J. S. (2014a) In situ produced branched glycerol dialkyl glycerol tetraethers in suspended particulate matter from the Yenisei River, Eastern Siberia. *Geochim. Cosmochim. Acta* **125**, 476–491.

De Jonge C., Hopmans E. C., Zell C. I., Kim J. H., Schouten S. and Sinninghe Damsté J. S. (2014b) Occurrence and abundance of 6-methyl branched glycerol dialkyl glycerol tetraethers in soils: Implications for palaeoclimate reconstruction. *Geochim. Cosmochim. Acta* **141**, 97–112.

De Jonge C., Stadnitskaia A., Hopmans E. C., Cherkashov G., Fedotov A., Streletskaya I. D., Vasiliev A. A. and Sinninghe Damsté J. S. (2015) Drastic changes in the distribution of branched tetraether lipids in suspended matter and sediments from the Yenisei River and Kara Sea (Siberia): Implications for the use of brGDGT-based proxies in coastal marine sediments. *Geochim. Cosmochim. Acta* **165**, 200–225.

De Jonge C., Radujković D., Sigurdsson B. D., Weedon J. T., Janssens I. and Peterse F. (2019) Lipid biomarker temperature proxy responds to abrupt shift in the bacterial community composition in geothermally heated soils. *Org. Geochem.*. https://doi.org/10.1016/j.orggeochem.2019.07.006.

Dearing Crampton-Flood E., Peterse F., Munsterman D. and Sinninghe Damsté J. S. (2018) Using tetraether lipids archived in North Sea Basin sediments to extract North Western European Pliocene continental air temperatures. *Earth Planet. Sc. Lett.* **490**, 193–205.

Delgado-Baquerizo M., Maestre F. T., Reich P. B., Trivedi P., Osana Y., Liu Y. R., Hamonts K., Jeffries T. C. and Singh B. K. (2016) Carbon content and climate variability drive global soil bacterial diversity patterns. *Ecol. Monogr.* **86**(3), 373–390.

Delgado-Baquerizo M., Bissett A., Eldridge D. J., Maestre F. T., He J. Z., Wang J. T., Hamonts K., Liu Y. R., Singh B. K. and Fierer N. (2017) Palaeoclimate explains a unique proportion of the global variation in soil bacterial communities. *Nat. Ecol. Evol.* **1**(9), 1339.

Deng L., Jia G., Jin C. and Li S. (2016) Warm season bias of branched GDGT temperature estimates causes underestimation of altitudinal lapse rate. *Org. Geochem.* **96**, 11–17.

Ding S., Xu Y., Wang Y., He Y., Hou J., Chen L. and He J. S. (2015) Distribution of branched glycerol dialkyl glycerol tetraethers in surface soils of the Qinghai-Tibetan Plateau: implications of brGDGTs-based proxies in cold and dry regions. *Biogeosciences* **12**(11), 3141–3151.

Dirghangi S. S., Pagani M., Hren M. T. and Tipple B. J. (2013) Distribution of glycerol dialkyl glycerol tetraethers in soils from two environmental transects in the USA. *Org. Geochem.* **59**, 49–60.

Drotz S. H., Sparrman T., Nilsson M. B., Schleucher J. and Öquist M. G. (2010) Both catabolic and anabolic heterotrophic microbial activity proceed in frozen soils. *P. Natl. Acad. Sci.* **107**(49), 21046–21051.

Frieling J., Iakovleva A. I., Reichart G. J., Aleksandrova G. N., Gnibidenko Z. N., Schouten S. and Sluijs A. (2014) Paleocene-Eocene warming and biotic response in the epicontinental West Siberian Sea. *Geology* **42**(9), 767–770.

Gelman A. (2003) A Bayesian formulation of exploratory data analysis and goodness-of-fit testing. *Int. Stat. Rev.* **71**(2), 369–382.

Grundstein A., Todhunter P. and Mote T. (2005) Snowpack control over the thermal offset of air and soil temperatures in eastern North Dakota. *Geophys. Res. Let.* **32**(8).

Harris I. P. D. J., Jones P. D., Osborn T. J. and Lister D. H. (2014) Updated high-resolution grids of monthly climatic observations–the CRU TS3. 10 Dataset. *Int. J. Climatology* **34**(3), 623–642.

Haywood A. M., Valdes P. J., Francis J. E. and Sellwood B. W. (2002) Global middle Pliocene biome reconstruction: A data/model synthesis. *Geochem. Geophy. Geosy.* **3**(12), 1–18.

Head M. J. (1998) Pollen and dinoflagellates from the Red Crag at Walton-on-the-Naze, Essex: evidence for a mild climatic phase during the early Late Pliocene of eastern England. *Geol. Mag.* **135**(6), 803–817.

Hollis C. J., Taylor K. W., Handley L., Pancost R. D., Huber M., Creech J. B., Hines B. R., Crouch E. M., Morgans H. E., Crampton J. S. and Gibbs S. (2012) Early Paleogene temperature history of the Southwest Pacific Ocean: Reconciling proxies and models. *Earth Planet. Sc. Lett.* **349**, 53–66.

Hopmans E. C., Schouten S. and Sinninghe Damsté J. S. (2016) The effect of improved chromatography on GDGT-based palaeoproxies. *Org. Geochem.* **93**, 1–6.

Huguet C., Hopmans E. C., Febo-Ayala W., Thompson D. H., Sinninghe Damsté J. S. and Schouten S. (2006) An improved method to determine the absolute abundance of glycerol dibiphytanyl glycerol tetraether lipids. *Org. Geochem.* **37**(9), 1036–1041.

Huguet A., Francez A. J., Jusselme M. D., Fosse C. and Derenne S. (2014) A climatic chamber experiment to test the short term effect of increasing temperature on branched GDGT distribution in Sphagnum peat. *Org. Geochem.* **73**, 109–112.

Inglis G. N., Farnsworth A., Lunt D., Foster G. L., Hollis C. J., Pagani M., Jardine P. E., Pearson P. N., Markwick P., Galsworthy A. M. and Raynham L. (2015) Descent toward the Icehouse: Eocene sea surface cooling inferred from GDGT distributions. *Paleoceanogr. Paleoclim.* **30**(7), 1000–1020.

Inglis G. N., Collinson M. E., Riegel W., Wilde V., Farnsworth A., Lunt D. J., Valdes P., Robson B. E., Scott A. C., Lenz O. K. and Naafs B. D. A. (2017) Mid-latitude continental temperatures through the early Eocene in western Europe. *Earth Planet. Sc. Lett.* **460**, 86–96.

Lauber C. L., Hamady M., Knight R. and Fierer N. (2009) Pyrosequencing-based assessment of soil pH as a predictor of soil bacterial community structure at the continental scale. *Appl. Environ. Microb.* **75**(15), 5111–5120.

Lei Y., Yang H., Dang X., Zhao S. and Xie S. (2016) Absence of a significant bias towards summer temperature in branched tetraether-based paleothermometer at two soil sites with contrasting temperature seasonality. *Org. Geochem.* **94**, 83–94.

Martínez-Sosa P. and Tierney J. E. (2019) Lacustrine brGDGT response to microcosm and mesocosm incubations. *Org. Geochem.* **127**, 12–22.

Menges J., Huguet C., Alcañiz J. M., Fietz S., Sachse D. and Rosell-Melé A. (2014) Influence of water availability in the

distributions of branched glycerol dialkyl glycerol tetraether in soils of the Iberian Peninsula. *Biogeosciences* **11**(10), 2571.

Naafs B. D. A., Gallego-Sala A. V., Inglis G. N. and Pancost R. D. (2017a) Refining the global branched glycerol dialkyl glycerol tetraether (brGDGT) soil temperature calibration. *Org. Geochem.* **106**, 48–56.

Naafs B. D. A., Inglis G. N., Zheng Y., Amesbury M. J., Biester H., Bindler R., Blewett J., Burrows M. A., del Castillo Torres D., Chambers F. M. and Cohen A. D. (2017b) Introducing global peat-specific temperature and pH calibrations based on brGDGT bacterial lipids. *Geochim. Cosmochim. Acta* **208**, 285–301.

Nedwell D. B. (1999) Effect of low temperature on microbial growth: lowered affinity for substrates limits growth at low temperature. *FEMS Microbiol. Ecol.* **30**(2), 101–111.

Oliverio A. M., Bradford M. A. and Fierer N. (2017) Identifying the microbial taxa that consistently respond to soil warming across time and space. *Global Change Biol.* **23**(5), 2117–2129.

Peterse F., Kim J. H., Schouten S., Kristensen D. K., Koç N. and Sinninghe Damsté J. S. (2009a) Constraints on the application of the MBT/CBT palaeothermometer at high latitude environments (Svalbard, Norway). *Org. Geochem.* **40**(6), 692–699.

Peterse F., Schouten S., van der Meer J., van der Meer M. T. and Sinninghe Damsté J. S. (2009b) Distribution of branched tetraether lipids in geothermally heated soils: implications for the MBT/CBT temperature proxy. *Org. Geochem.* **40**(2), 201–205.

Peterse F., Nicol G. W., Schouten S. and Sinninghe Damsté J. S. (2010) Influence of soil pH on the abundance and distribution of core and intact polar lipid-derived branched GDGTs in soil. *Org. Geochem.* **41**(10), 1171–1175.

Peterse F., Prins M. A., Beets C. J., Troelstra S. R., Zheng H., Gu Z., Schouten S. and Sinninghe Damsté J. S. (2011) Decoupled warming and monsoon precipitation in East Asia over the last deglaciation. *Earth Planet. Sc. Lett.* **301**(1–2), 256–264.

Peterse F., van der Meer J., Schouten S., Weijers J. W., Fierer N., Jackson R. B., Kim J. H. and Sinninghe Damsté J. S. (2012) Revised calibration of the MBT–CBT paleotemperature proxy based on branched tetraether membrane lipids in surface soils. *Geochim. Cosmochim Acta* **96**, 215–229.

Pope V. D., Gallani M. L., Rowntree P. R. and Stratton R. A. (2000) The impact of new physical parametrizations in the Hadley Centre climate model: HadAM3. *Clim. Dynam.* **16**(2–3), 123–146.

Pross J. and Klotz S. (2002) Palaeotemperature calculations from the Praetiglian/Tiglian (Plio–Pleistocene) pollen record of Lieth, northern Germany: implications for the climatic evolution of NW Europe. *Global Planet. Change* **34**(3–4), 253–267.

Rueda G., Rosell-Melé A., Escala M., Gyllencreutz R. and Backman J. (2009) Comparison of instrumental and GDGT-based estimates of sea surface and air temperatures from the Skagerrak. *Org. Geochem.* **40**(2), 287–291.

Salzmann U., Haywood A. M., Lunt D. J., Valdes P. J. and Hill D. J. (2008) A new global biome reconstruction and data-model comparison for the middle Pliocene. *Global Ecol. Biogeogr.* **17**(3), 432–447.

Schostag M., Stibal M., Jacobsen C. S., Bælum J., Taş N., Elberling B., Jansson J. K., Semenchuk P. and Priemé A. (2015) Distinct summer and winter bacterial communities in the active layer of Svalbard permafrost revealed by DNA-and RNA-based analyses. *Front. Microbiol.* **6**, 399.

Sinninghe Damsté J. S., Hopmans E. C., Pancost R. D., Schouten S. and Geenevasen J. A. (2000) Newly discovered non-isoprenoid glycerol dialkyl glycerol tetraether lipids in sediments. *Chem. Comms.* **17**, 1683–1684.

Sinninghe Damsté J. S., Ossebaar J., Schouten S. and Verschuren D. (2008) Altitudinal shifts in the branched tetraether lipid distribution in soil from Mt. Kilimanjaro (Tanzania): Implications for the MBT/CBT continental palaeothermometer. *Org. Geochem.* **39**(8), 1072–1076.

Sinninghe Damsté J. S., Ossebaar J., Abbas B., Schouten S. and Verschuren D. (2009) Fluxes and distribution of tetraether lipids in an equatorial African lake: constraints on the application of the TEX86 palaeothermometer and BIT index in lacustrine settings. *Geochim. Cosmochim. Acta* **73**(14), 4232–4249.

Sinninghe Damsté J. S., Rijpstra W. I. C., Hopmans E. C., Weijers J. W., Foesel B. U., Overmann J. and Dedysh S. N. (2011) 13, 16-Dimethyl octacosanedioic acid (iso-diabolic acid), a common membrane-spanning lipid of Acidobacteria subdivisions 1 and 3. *Appl. Env. Microbiol.* **77**(12), 4147–4154.

Sinninghe Damsté J. S. (2016) Spatial heterogeneity of sources of branched tetraethers in shelf systems: The geochemistry of tetraethers in the Berau River delta (Kalimantan, Indonesia). *Geochim. Cosmochim. Acta* **186**, 13–31.

Sinninghe Damsté J. S., Rijpstra W. I. C., Foesel B. U., Huber K. J., Overmann J., Nakagawa S., Kim J. J., Dunfield P. F., Dedysh S. N. and Villanueva L. (2018) An overview of the occurrence of ether-and ester-linked iso-diabolic acid membrane lipids in microbial cultures of the Acidobacteria: Implications for brGDGT paleoproxies for temperature and pH. *Org. Geochem.* **124**, 63–76.

Suc J. and Zagwijn W. H. (1983) Plio-Pleistocene correlations between the northwestern Mediterranean region and northwestern Europe according to recent biostratigraphic and palaeoclimatic data. *Boreas* **12**, 153–166.

Tierney J. E. and Russell J. M. (2009) Distributions of branched GDGTs in a tropical lake system: implications for lacustrine application of the MBT/CBT paleoproxy. *Org. Geochem.* **40**(9), 1032–1036.

Tierney J. E. and Tingley M. P. (2014) A Bayesian, spatially-varying calibration model for the TEX 86 proxy. *Geochim. Cosmochim. Acta* **127**, 83–106.

Tierney J. E. and Tingley M. P. (2018) BAYSPLINE: a new calibration for the alkenone paleothermometer. *Paleoceanogr. Paleoclim.* **33**(3), 281–301.

Uhl D., Klotz S., Traiser C., Thiel C., Utescher T., Kowalski E. and Dilcher D. L. (2007) Cenozoic paleotemperatures and leaf physiognomy—a European perspective. *Palaeogeogr. Palaeocl.* **248**(1–2), 24–31.

Utescher T., Mosbrugger V. and Ashraf A. R. (2000) Terrestrial climate evolution in northwest Germany over the last 25 million years. *Palaios* **15**(5), 430–449.

Wang H., Liu W. and Lu H. (2016) Appraisal of branched glycerol dialkyl glycerol tetraether-based indices for North China. *Org. Geochem.* **98**, 118–130.

Warden L., Moros M., Weber Y. and Sinninghe Damsté J. S. (2018) Change in provenance of branched glycerol dialkyl glycerol tetraethers over the Holocene in the Baltic Sea and its impact on continental climate reconstruction. *Org. Geochem.* **121**, 138–154.

Weber Y., De Jonge C., Rijpstra W. I. C., Hopmans E. C., Stadnitskaia A., Schubert C. J., Lehmann M. F., Sinninghe Damsté J. S. and Niemann H. (2015) Identification and carbon isotope composition of a novel branched GDGT isomer in lake sediments: Evidence for lacustrine branched GDGT production. *Geochim. Cosmochim. Acta* **154**, 118–129.

Weber Y., Sinninghe Damsté J. S., Zopfi J., De Jonge C., Gilli A., Schubert C. J., Lepori F., Lehmann M. F. and Niemann H. (2018) Redox-dependent niche differentiation provides evidence

for multiple bacterial sources of glycerol tetraether lipids in lakes. *P. Natl. Acad. Sci.* **115**(43), 10926–10931.

Weijers J. W., Schouten S., Hopmans E. C., Geenevasen J. A., David O. R., Coleman J. M., Pancost R. D. and Sinninghe Damsté J. S. (2006) Membrane lipids of mesophilic anaerobic bacteria thriving in peats have typical archaeal traits. *Env. Microbiol.* **8**(4), 648–657.

Weijers J. W., Schouten S., van den Donker J. C., Hopmans E. C. and Sinninghe Damsté J. S. (2007a) Environmental controls on bacterial tetraether membrane lipid distribution in soils. *Geochim. Cosmochim. Acta* **71**(3), 703–713.

Weijers J. W., Schefuß E., Schouten S. and Sinninghe Damsté J. S. (2007b) Coupled thermal and hydrological evolution of tropical Africa over the last deglaciation. *Science* **315**(5819), 1701–1704.

Weijers J. W., Schouten S., Sluijs A., Brinkhuis H. and Sinninghe Damsté J. S. (2007c) Warm arctic continents during the Palaeocene-Eocene thermal maximum. *Earth Planet. Sc. Let.* **261**(1–2), 230–238.

Weijers J. W., Panoto E., van Bleijswijk J., Schouten S., Rijpstra W. I. C., Balk M., Stams A. J. and Sinninghe Damsté J. S. (2009) Constraints on the biological source (s) of the orphan branched tetraether membrane lipids. *Geomicrobiol. J.* **26**(6), 402–414.

Weijers J. W. H., Wiesenberg G. L., Bol R., Hopmans E. C. and Pancost R. D. (2010) Carbon isotopic composition of branched tetraether membrane lipids in soils suggest a rapid turnover and a heterotrophic life style of their source organism (s). *Biogeosciences* **7**(9), 2959–2973.

Weijers J. W., Bernhardt B., Peterse F., Werne J. P., Dungait J. A., Schouten S. and Sinninghe Damsté J. S. (2011) Absence of seasonal patterns in MBT–CBT indices in mid-latitude soils. *Geochim. Cosmochim. Acta* **75**(11), 3179–3190.

Wilf P. (2000) Late Paleocene–early Eocene climate changes in southwestern Wyoming: Paleobotanical analysis. *Geolog. Soc. America Bull.* **112**(2), 292–307.

Xiao W., Xu Y., Ding S., Wang Y., Zhang X., Yang H., Wang G. and Hou J. (2015) Global calibration of a novel, branched GDGT-based soil pH proxy. *Org. Geochem.* **89**, 56–60.

Yang H., Lü X., Ding W., Lei Y., Dang X. and Xie S. (2015) The 6-methyl branched tetraethers significantly affect the performance of the methylation index (MBT′) in soils from an altitudinal transect at Mount Shennongjia. *Org. Geochem.* **82**, 42–53.

Zagwijn W. H. (1963) Pollen-analytic investigations in the Tiglian of the Netherlands. *Geol. Stichting Meded.* **16**, 49–69.

Zell C., Kim J. H., Moreira-Turcq P., Abril G., Hopmans E. C., Bonnet M. P., Sobrinho R. L. and Sinninghe Damsté J. S. (2013a) Disentangling the origins of branched tetraether lipids and crenarchaeol in the lower Amazon River: Implications for GDGT-based proxies. *Limnol. Oceanogr.* **58**, 343–353.

Zell C., Kim J. H., Abril G., Sobrinho R., Dorhout D., Moreira-Turcq P. and Sinninghe Damsté J. (2013b) Impact of seasonal hydrological variation on the distributions of tetraether lipids along the Amazon River in the central Amazon basin: implications for the MBT/CBT paleothermometer and the BIT index. *Front. Micro.* **4**, 228.

Zell C., Kim J. H., Hollander D., Lorenzoni L., Baker P., Silva C. G., Nittrouer C. and Sinninghe Damsté J. S. (2014a) Sources and distributions of branched and isoprenoid tetraether lipids on the Amazon shelf and fan: Implications for the use of GDGT-based proxies in marine sediments. *Geochim. Cosmochim. Acta* **139**, 293–312.

Zell C., Kim J. H., Balsinha M., Dorhout D., Fernandes C., Baas M. and Sinninghe Damsté J. S. (2014b) Transport of branched tetraether lipids from the Tagus River basin to the coastal ocean of the Portuguese margin: consequences for the interpretation of the MBT'/CBT paleothermometer. *Biogeosciences* **11**, 5637–5655.

Associate Editor: Elizabeth Ann Canuel